

Chapter 8

Advanced Combustion in Natural Gas-Fueled Engines



Ulugbek Azimov , Nobuyuki Kawahara , Kazuya Tsuboi 
and Eiji Tomita 

Abstract Current energy and emission regulations set the requirements to increase the use of natural gas in engines for transportation and power generation. The characteristics of natural gas are high octane number, less amount of carbon in the molecule, suitable to lean combustion, less ignitibility, etc. There are some advantages of using natural gas for engine combustion. First, less carbon dioxide is emitted due to its molecular characteristics. Second, higher thermal efficiency is achieved owing to the high compression ratio compared to that of gasoline engines. Natural gas has higher octane number so that knock is hard to occur even at high compression ratios. However, this becomes a disadvantage in homogeneous charge compression ignition (HCCI) engines or compression ignition engines because the initial auto-ignition is difficult to be achieved. When natural gas is used in a diesel engine, primary natural gas–air mixture is ignited with small amount of diesel fuel. It was found that under high pressure, lean conditions, and with the control of certain parameters, the end gas is auto-ignited without knock and improves the engine combustion efficiency. Recently, some new fuel ignition technologies have been developed to be applied to natural gas engines. These are the laser-assisted and plasma-assisted ignition systems with high energy and compact size.

Keywords Natural gas IC engine · Dual-fuel engine · HCCI · RCCI
Laser-assisted ignition · Plasma-assisted ignition · PREMIER

U. Azimov (✉)

University of Northumbria, Newcastle upon Tyne NE1 8ST, UK
e-mail: ulugbek.azimov@northumbria.ac.uk

N. Kawahara · K. Tsuboi · E. Tomita
Okayama University, Tsushima-Naka 3, Okayama 700-8530, Japan

Abbreviations

ATDC	After top dead center
AFR	Air–fuel ratio
BTDC	Before top dead center
CA	Crank angle
CAD	Crank angle degree
CFD	Computational fluid dynamics
CI	Compression ignition
CNG	Compressed natural gas
CO	Carbon monoxide
CO ₂	Carbon dioxide
EVC	Exhaust valve closing
EVO	Exhaust valve opening
EGR	Exhaust gas recirculation
ϕ	Equivalence ratio
IMEP	Indicated mean effective pressure
IVC	Intake valve close
IVO	Intake valve open
HC	Hydrocarbon
HCCI	Homogeneous charge compression ignition
HRR	Heat release rate
IC	Internal combustion
LES	Large Eddy simulation
LTC	Low-temperature combustion
m_{DF}	Mass of pilot-injected diesel fuel
NG	Natural gas
NO	Nitrogen monoxide
NO _x	Nitrogen oxides
P	Pressure
PCCI	Premixed charge compression ignition
rpm	Revolution per minute
RANS	Reynolds-averaged Navier–Stokes
RCCI	Reactivity controlled compression ignition
SI	Spark ignition
SOC	Start of combustion
SOI	Start of injection
T	Temperature
T_G	Ignition temperature
TDC	Top dead center
UHC	Unburned hydrocarbon
V	Volume

8.1 Introduction

Internal combustion (IC) engines can perform more efficiently and with a lower level of toxic emissions if natural gas (NG) is used as a fuel. NG is a naturally occurring gas mixture, which consists of primarily methane and some amount of higher hydrocarbons, nitrogen, and carbon dioxide. Typical composition of a commercial NG product is shown in Fig. 8.1.

Due to the lowest carbon-to-hydrogen ratio, compared to other fossil fuels, NG emits the least amount of CO_2 during its combustion. Plentiful resources, lower price, and cleaner burning compared to conventional liquid fuels have made NG a very economic fuel to be used in IC engines. Another important feature of NG, its high octane number, makes it suitable to be used in engines with high compression ratios (Zheng et al. 2005).

To meet low emission standards for IC engines, researchers have been extensively studying the low-temperature combustion (LTC) concept (Dempsey et al. 2014; Caton 2011). These studies showed that utilizing LTC strategies in engines can result in a simultaneous reduction of nitrogen oxides (NO_x) and soot emissions and also helps achieving higher thermal efficiencies (Jia et al. 2011; Asad et al. 2013; Aoyama et al. 1996).

NG can be also used in a homogeneous charge compression ignition (HCCI) engines. In the HCCI combustion mode, a mixture of air and NG is auto-ignited due

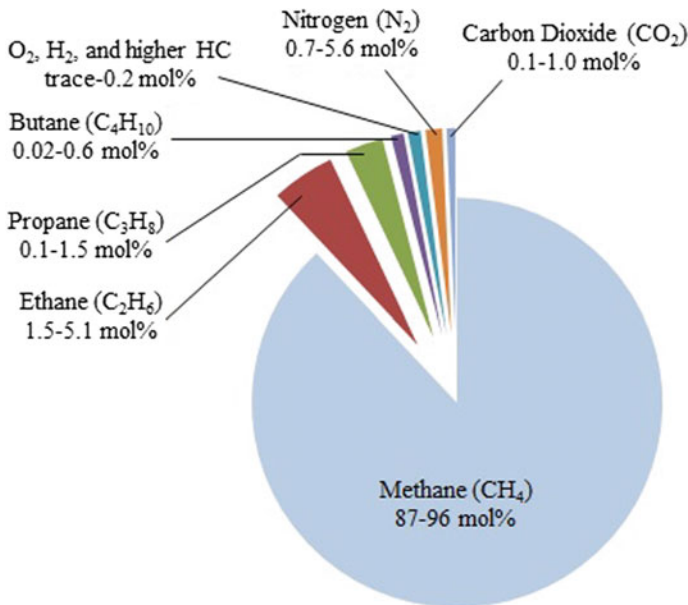


Fig. 8.1 Typical composition of a commercial NG product (<http://www.uniongas.com/aboutus/aboutng/composition.asp>)

to the temperature increase close to the top dead center (TDC). The combustion process is significantly faster than that in either traditional compression ignition (CI) or spark ignition (SI) engines (Reitz 2013). The challenge for HCCI engine is to control auto-ignition and combustion. A new LTC concept named reactivity controlled compression ignition (RCCI) was developed by the researchers (Kokjohn et al. 2010, 2011; Splitter et al. 2010) to overcome difficulties like combustion phasing control and very high pressure rise rate (PRR), to extend engine operating limits and avoid potential combustion instability and misfire (Imtenan et al. 2014; Gharehghani et al. 2015; Zhou et al. 2015; Benajes et al. 2015; Li et al. 2015; Laguitton et al. 2007; Molina et al. 2015; Nieman et al. 2012; Paykani et al. 2015; Kakaee et al. 2015; Christensen and Johansson 1998).

The demand for high thermal efficiency can be met through ignition of lean fuel mixtures. However, lean combustion is related to slower flame propagation speeds and decreased power output. Engine power output can be elevated through boosting the initial cylinder pressure. An increase in the cylinder pressure keeping the same spark plug electrode distance would require increased secondary coil voltage, which leads to extreme erosion of electrodes over time. Flame propagation speed in lean air–fuel mixtures can be expanded whether through optimizing the position of ignition spot in the combustion chamber or with the aid of multi-point ignition. Ignition spot always stays close to the top of the combustion chamber in a traditional spark ignition engine and cannot be varied from its location. This can be resolved by using a laser as an ignition source.

In addition to the laser ignition, the possible use of non-equilibrium plasma for ignition and combustion control has also raised the increasing interest due to the possibility of plasma-assisted approaches for ignition and flame stabilization. During the past decade, significant progress has been made toward understanding the mechanisms of plasma–chemistry interactions, power redistribution, and the non-equilibrium initiation of combustion (Starikovskii 2005). Plasma application has been shown to furnish additional combustion control, which is crucial for ultra-lean flames, high-speed flows, high-pressure conditions, and distributed ignition control in HCCI engines. In addition, a wide variety of fuels have been examined for the use of various types of discharge plasmas. The following sections will describe in more detail the above-mentioned combustion and ignition technologies and techniques applied for natural gas-fueled engines.

8.2 Combustion of Natural Gas in Dual-Fuel Engines

To meet stringent emission standards, researchers have been developing LTC solutions to improve the traditional internal combustion engines in order to develop IC engines with higher efficiencies and cleaner combustion (Agarwal et al. 2017; Musculus Mark et al. 2013; Gharehghani et al. 2016; Scott Guerry et al. 2016).

Many different gaseous and liquid fuels have been evaluated in the dual-fuel combustion engine, and natural gas is believed to be one of the most suitable alternatives due to the low cost and excellent antiknock properties (Wagemakers and Leermakers 2012; Hosmath et al. 2016).

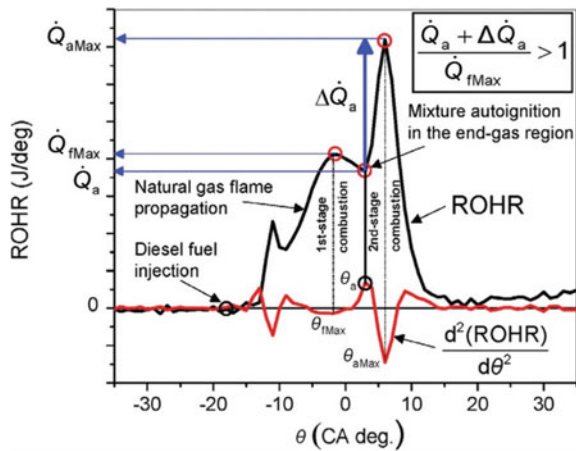
8.2.1 Experimental Research on Dual-Fuel Engines

Several experimental research efforts on dual-fuel engines were carried out by the authors of this chapter. The more detailed explanation can be found in references (Tomita et al. 2002, 2004, 2007; Roy et al. 2009). Tomita et al. (2009) investigated the combustion and exhaust emissions in supercharged dual-fuel natural gas engines. The authors documented the range of operating conditions under which the new higher efficiency **PREM**ixed **MIX**ture **IGN**ition in the **EN**d-**GA**s **R**egion (PREMIER) combustion mode was experimentally tested in a pilot-ignited, natural gas dual-fuel engine. The heat release during the PREMIER combustion is presented in Fig. 8.2. The details of this combustion mode are presented in the reference (Tomita et al. 2009).

Figure 8.3 shows a schematic diagram of the experimental setup. The engine specifications and experimental conditions are given in Table 8.1 and explained in detail in the reference (Tomita et al. 2009).

Figure 8.4 shows the flame development of NG as a primary fuel ignited by micro-pilot-ignited diesel fuel. The flame area is gradually increasing in all four directions with the flame front finally reaching the cylinder wall. The flame speed is affected by the CO and CO₂ gases produced during the combustion. The effect of these species on fuel oxidation and flame propagation is a quite complex topic and is outside of the scope of this chapter. Figure 8.5 shows the intensity of the emitted

Fig. 8.2 Conceptual illustration of PREMIER combustion as the rate of heat release



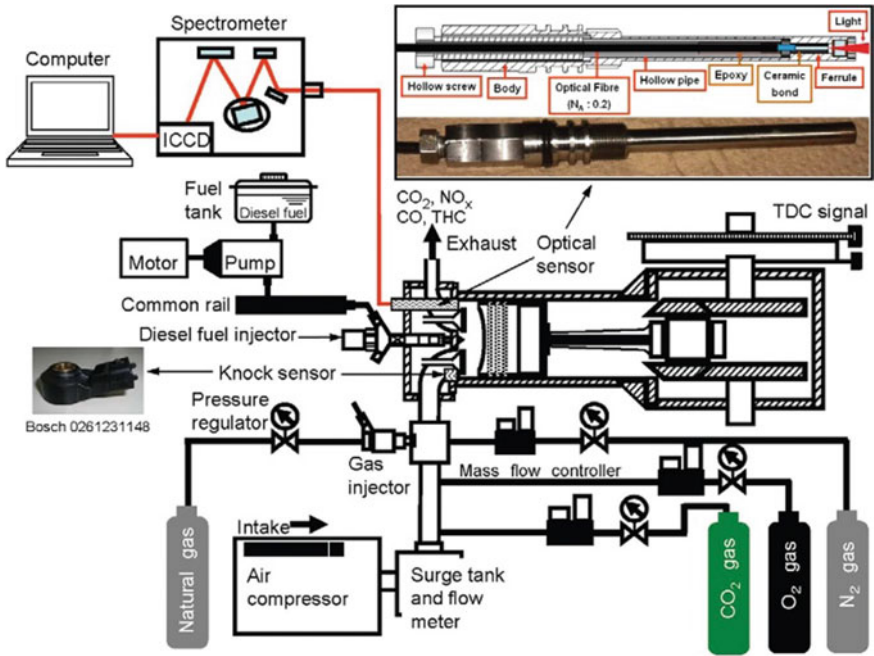


Fig. 8.3 Schematic diagram of experimental setup

Table 8.1 Engine specification and experimental conditions

Engine type	Four stroke, single cylinder, water cooled
Bore × stroke	96 × 108 mm
Swept volume	781.7 cm ³
Compression ratio	16
Combustion system	Dual fuel, direct injection
Combustion chamber	Shallow dish
Engine speed	1000 r/min
Intake pressure	101, 200 kPa
Injection system	Common rail
Nozzle hole × diameter	3 × 0.10 mm, 3 × 0.08 mm, 4 × 0.10 mm
Pilot fuel injection pressure	40, 80, 120, 150 MPa
Pilot fuel injection quantity	2, 3 mg/cycle
Injection timing	From 13° BTDC to TDC
Equivalence ratio	0.6

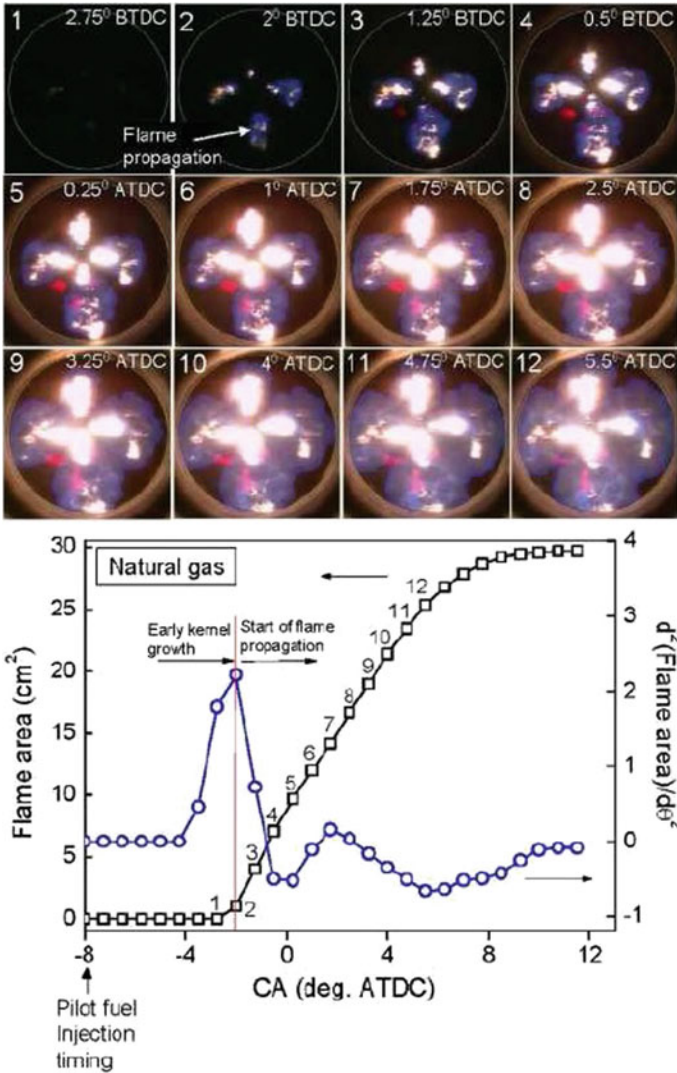
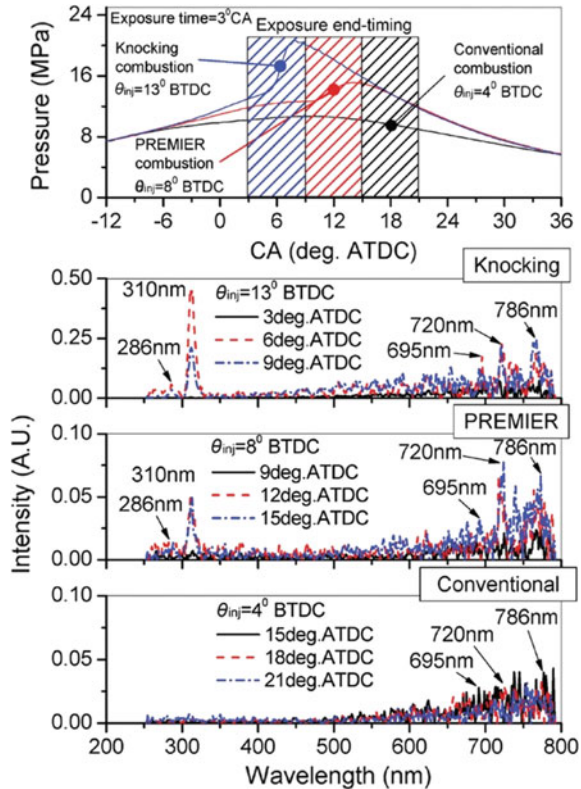


Fig. 8.4 Dual-fuel combustion sequential images at $P_{inj} = 40$ MPa, $P_{in} = 101$ kPa, $\theta_{inj} = 8^\circ$ BTDC, $m_{DF} = 2$ mg/cycle, $\phi_t = 0.6$. Natural gas, $CH_4 = 88\%$, $C_2H_6 = 6\%$, $C_3H_8 = 4\%$, $n-C_4H_{10} = 2\%$

light as background-subtracted ensemble-averaged spectra at the instances the propagating flame arrives at the end-gas region where the optical sensor is installed to capture the end-gas region auto-ignition. The detailed explanations of this setup are provided in the reference (Azimov et al. 2011).

Fig. 8.5 Detailed spectra in the end-gas region.
 $P_{inj} = 40$ MPa,
 $P_{in} = 200$ kPa,
 $D_{hole} = 0.1$ mm, $N_{hole} = 3$,
 $m_{DF} = 2$ mg/cycle



To maintain PREMIER combustion in a dual-fuel natural gas engine, the effects of several operating parameters must be identified. For example, as shown in Fig. 8.6, PREMIER combustion can be achieved by maintaining certain fixed experimental conditions (Azimov et al. 2016).

The engine experimental conditions are presented in Table 8.2.

8.2.2 Numerical Modeling of Dual-Fuel Engines

Dual-fuel combustion is one of the efficient, clean yet difficult to model phenomenon. Dual-fuel combustion has both CI and SI characteristics in addition to its own typical behavior, which increases the complexity of the combustion process. Traditionally, in the dual-fuel combustion process, a diesel spray is introduced in a nearly homogeneous air–fuel mixture. To model dual-fuel combustion, the well-established auto-ignition models can be used. As the first stage of the dual-fuel combustion is auto-ignition, these models can be applied directly without any change under the assumption that diesel auto-ignition is not affected by the presence

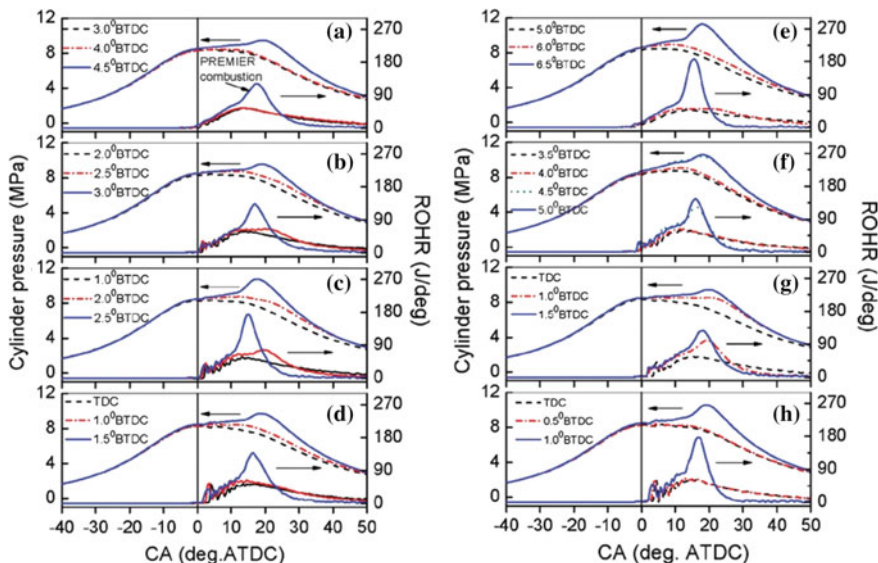


Fig. 8.6 Effect of pilot fuel injection timing on cylinder pressure and the rate of heat release

Table 8.2 Engine experimental conditions

	P_{inj} (MPa)	P_{in} (kPa)	D_{hole} (mm)	N_{hole}	m_{DF} (mg/cycle)
a	40	200	0.1	3	3
b	80	200	0.1	3	3
c	120	200	0.1	3	3
d	150	200	0.1	3	3
e	40	200	0.1	3	2
f	80	200	0.1	3	2
g	150	200	0.08	3	3
h	150	200	0.1	4	3

of another fuel species such as methane, and traces of ethane, propane, and iso-butane. In reality, traces of any gaseous fuel can change ignition delay, temperature of auto-ignition process, duration of first-stage ignition, and laminar burning velocity. Hence, diesel substitution ratio is very important in order to recognize the percentage of energy delivered by diesel fuel.

One of the current challenges in the 3D CFD simulation of the dual-fuel combustion is to get the correct heat release from the chemical reactions compared with the experimental data. This is important to predict knock in the dual-fuel operation. Dual-fuel engine starts combustion using pilot fuel spray, and auto-ignition of that small fuel acts as a spark energy for the lean gaseous fuel-air mixture. This mode of combustion can be investigated experimentally as was explained in earlier section,

but poses a very complicated problem for 3D CFD modeling. In SI engines, spark location is known and has precise spark energy, spark efficiency, and duration of the spark associated with it whereas dual-fuel engine heavily depends on the nature of the pilot spray to start premixed flame-type combustion.

The sequence of different types of combustion is very important for dual-fuel operation mode. For regular dual-fuel operation, the diesel pilot spray evaporates and mixes with already almost homogeneous mixture of natural gas and air. During this process, auto-ignition of diesel takes place and produces first heat release. This rate of heat release heavily depends on the quantity of diesel, compression ratio, and local equivalence ratio. First ignition starts the flame propagation and consumes most of the gaseous fuel. It is important to focus on the end-gas ignition, which follows the traditional flame propagation and has significant heat release rate compared to the first two zones, namely auto-ignition of diesel and flame front propagation in lean NG–air mixture. Hence, auto-ignition model with detailed chemistry and well-established flame propagation model hereafter mentioned as G-equation model can be used to model dual-fuel combustion in diesel engine. G-equation model is:

$$\frac{\partial \rho G}{\partial t} + \frac{\partial \rho \hat{u}_i G}{\partial x_i} = -D_t \kappa \left| \frac{\partial G}{\partial x_i} \right| + \rho_u S_t \left| \frac{\partial G}{\partial x_i} \right| \quad (8.1)$$

where D_t is turbulent diffusion, κ is curvature of the flame, ρ_u is unburnt density, and S_t is turbulent flame speed. Depending on the fuel composition and local equivalence ratio, ignition temperature is found to vary between 950 and 1100 K and hereafter it is denoted by T_G . This temperature (T_G) was decided using 0D auto-ignition model for homogeneous charge in CHEMKIN. T_G changes per local equivalence ratio and fuel composition. El Merhubi et al. (2016) conducted high-pressure (40 bar) methane auto-ignition using shock tube and also validated GRI 3.0 mechanism for $\phi = 0.5$ –1.0. At 40 bar pressure, auto-ignition temperature of methane ($\phi = 0.5$) is 1560 K. Though HCCI calculations assume premixed charge, it is important to note that 1% diesel quantity by energy content significantly changes auto-ignition temperature of methane. If n -heptane mass fraction is less than 0.021, then T_G is on the higher side. Hence, the value of T_G needs to be determined each time when the fuel composition changes. S_t is derived from laminar flame speed S_l , when used for RANS modeling; it includes u' root mean square of turbulent fluctuation velocity as shown in Eq. 8.2 (Peters 2000).

$$S_t = S_l + u' \left(\left(\frac{-a_4 b_3^2}{2b_1} D_a \right) + \left[\left(\frac{-a_4 b_3^2}{2b_1} D_a \right)^2 + a_4 b_3^2 D_a \right]^{\frac{1}{2}} \right) \quad (8.2)$$

where $b_1 = 2.0$, $b_3 = 1.0$, $a_4 = 0.78$, D_a —Damkohler number.

Equation 8.3 derived by Pitch (2002) is used for LES cases to calculate S_t

$$S_t = S_l \left(\left(\frac{-b_3^2 C_s \Delta}{2b_1 S_c l_F} \right) + \sqrt{\left(\frac{b_3^2 C_s \Delta}{2b_1 S_c l_F} \right)^2 + \frac{b_3^2 D_t}{S_l l_F} + 1} \right) \quad (8.3)$$

where S_c is turbulent Schmidt number, Δ is the filter width, and C_s is dynamic Smagorinsky number. In G -equation model $G(x, t)$ is a non-reactive scalar iso-surface for any fixed value of x . The flame front is described by $G = 0$ surface, and the flame thickness is superimposed by G' on this iso-surface. G -equation depends on the closure solution for calculating turbulent flame speed and does not have a source term; hence, G -equation model can be easily coupled with detailed chemistry model (Yang and Reitz 2010; Liang et al. 2007; Long 2006; Tamagna et al. 2008). Positive value of G suggests burnt zone, and negative value is used for unburnt zone. In the current model, laminar flame speed is calculated using CHEMKIN 1D laminar flame speed calculations instead of Guilder's equation (Gulder 1984) as it tends to overpredict the laminar flame speed for single component fuels like methane at high pressure and temperature conditions.

Figure 8.7 shows combustion progress at 4.5° BTDC after injection has occurred at 14.5° BTDC. Formaldehyde (CH_2O) is a main attribute of low-temperature combustion which appears not only in the vicinity of the flame kernels but on the peripheral area of entire combustion chamber. Plotted iso-surface at $G = 0.0001$ shows predominantly low-temperature regions. The empty region in the middle of combustion chamber is a high-temperature zone, and in the third figure, OH concentration is highest in the same region. This shows the smaller high-temperature region near spray surrounded by cluster of low-temperature ignition sites.

Figure 8.8 shows the development of the initial kernel after the second micro-pilot injection is complete. CH_2O iso-surface is created for highest concentration and colored by temperature to show the sites of preignition low-temperature chemistry. Subsequently, G iso-surface at value $1e-04$, i.e., at 0.1 mm distance from mean flame front inside the burn zone is also colored by temperature which shows three major kernel formation zones around three spray lobes. It is very important to note that outside the flame zone, at low-temperature initial kernel development starts at various locations. This kernel depending on the location from the wall and from mean flame front either becomes auto-ignition sites or just contributes to small energy release. OH iso-surface is plotted at highest mass fraction of OH ($1.e-03$) and shows the high-temperature chemistry inside the burnt zone. The heat release in case of the split micro-pilot injection is illustrated with CH_2O and G iso-surface as shown in Fig. 8.8 at 6° ATDC. The first micro-pilot injection occurs at 6° BTDC, and Fig. 8.8 shows the aftermath for flame kernel development after the second micro-pilot injection at 5° ATDC. The positive value of G suggests the burnt region, and the negative value shows the unburnt region outside the flame zone whereas $G = 0$ is the mean flame front brush. CH_2O and G -surfaces are colored by temperature to show low-temperature flame segments. $G = 1e-04$ shows the 0.1 mm zone inside the burnt zone after the flame front has

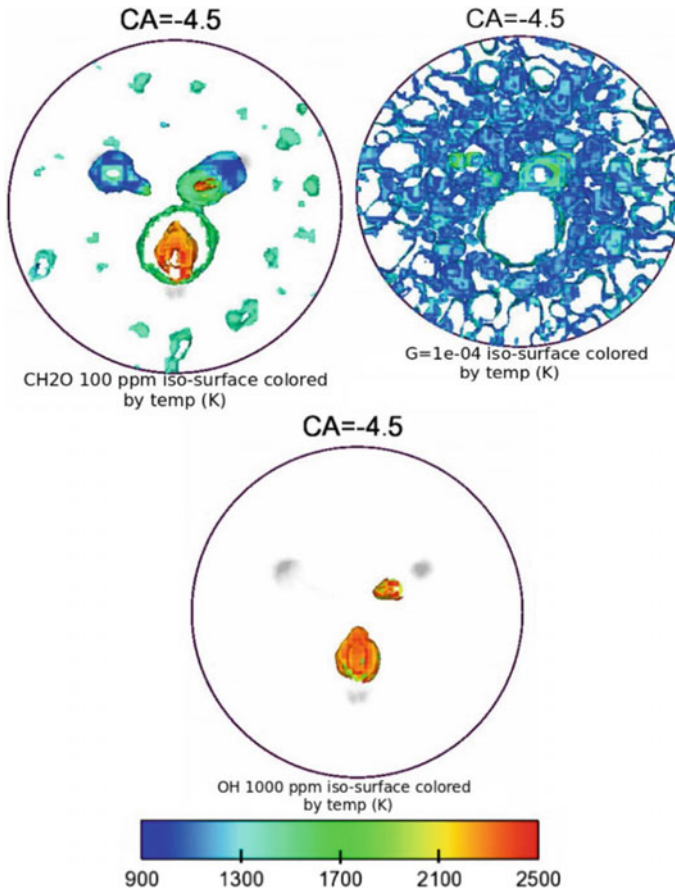


Fig. 8.7 CH₂O and G iso-surfaces for low-temperature flame localization, and OH for high-temperature combustion (single micro-pilot injected at 14.5° BTDC). RPM—1000, P_{inj} —40 MPa, CH₄—25 mg/cyl, diesel—0.8 mg/cyl, λ —1.92, IMEP—1.5 MPa

passed. CH₂O iso-surface shows in the pre-flame chemistry occurring outside the flame front at much lower temperature of 900 K, where inside the burnt zone the temperature is 2500 K.

Figure 8.9 shows trend of local temperature, which includes single micro-pilot injection at 14.5° BTDC. The highest temperature is noted from preheat region (1 mm away from the flame front), and second highest temperature belongs to the burnt region (1–2 mm inside the flame front). It is also important to note that around 6° BTDC mean flame front ($G = 0$) reaches highest temperature, and at the same time in preheat region 2–5 mm away from mean flame, there is a sudden increase in temperature. This is a very clear indication of end-gas ignition provided that temperature is much less at 0.5 mm outside the flame.

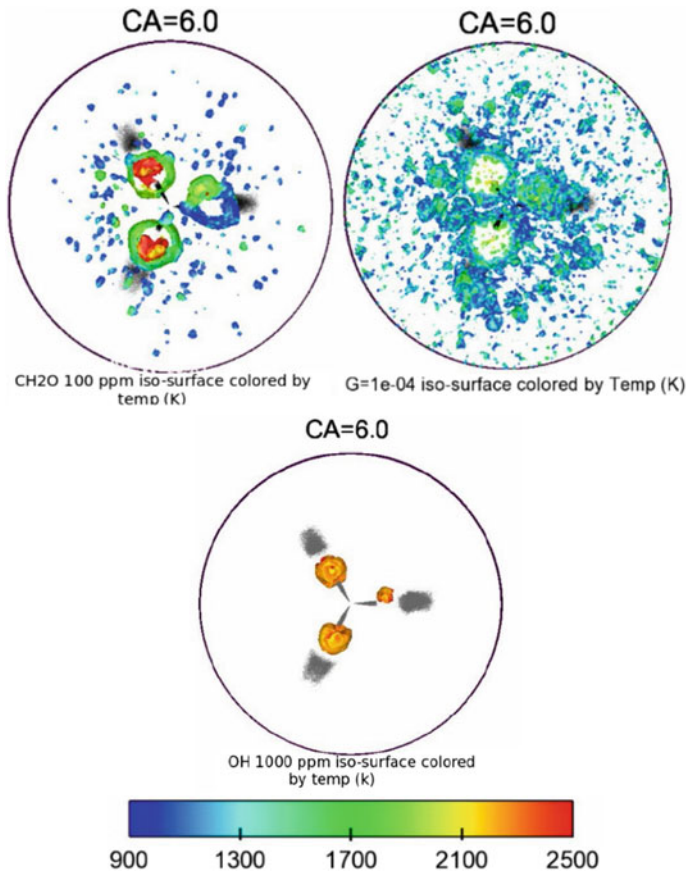


Fig. 8.8 CH₂O and G iso-surfaces for low-temperature flame localization, and OH for high-temperature combustion (the first micro-pilot injection is at 6° BTDC, and the second micro-pilot injection is at 5° ATDC). RPM—1000, P_{inj} —40 MPa, CH₄—26.7 mg/cyl, diesel inj—first (6° BTDC)—0.8 mg/cyl, second (5° ATDC)—0.8 mg/cyl, λ —1.66, IMEP—0.82 MPa

Figure 8.10 shows the local temperature and pressure data for the same scenario, and there are two major heat release zones; the first one is at 1000 K range, and the second zone shows high-temperature end-gas heat release at 2100 K range. Both LES and RANS turbulent models with the same combustion model showed good agreement in terms of end-gas ignition.

Figure 8.11 shows the gradient G that represents the temperature profiles in three combustion regions. The positive values of G represent the temperature in the burnt zone where post-flame chemistry is dominant and has the highest temperature in the combustion chamber. Negative values of G show the preheat or pre-flame regime where end-gas ignition happens in PREMIER cases. This is an excellent way of predicting temperature in the end-gas region instead of just observing few locations for higher heat release.

Fig. 8.9 Temperature profile for different G values with single micro-pilot injection. RPM—1000, P_{inj} —40 MPa, CH_4 —25 mg/cyl, diesel—0.8 mg/cyl, λ —1.92, IMEP—1.5 MPa

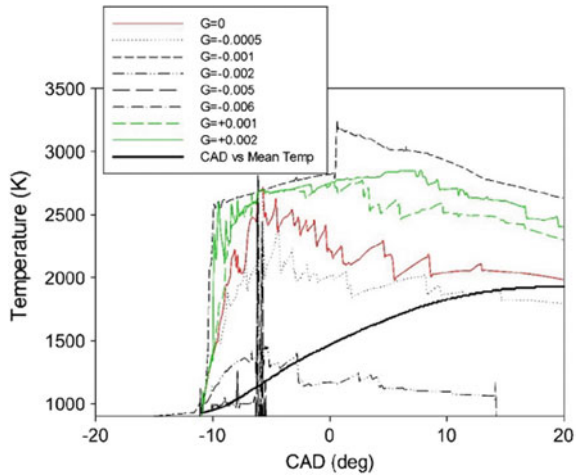


Fig. 8.10 Local temperature–pressure relationship with single micro-pilot injection. RPM—1000, P_{inj} —40 MPa, CH_4 —25 mg/cyl, diesel—0.8 mg/cyl, λ —1.92, IMEP—1.5 MPa

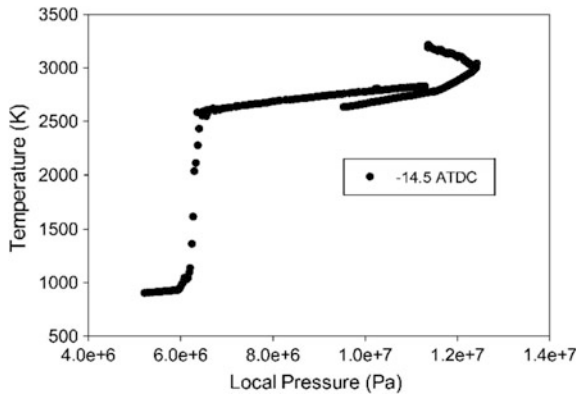


Figure 8.12 shows the effect of split micro-pilot injection. Ignition sites for split pilot injection are less in number compared to the single pilot injection case. The graph shows the effect of methane on the first ignition temperature as well as the overall temperature trend. For this case, when methane is present, first-stage ignition temperature is lower as compared to the scenario when methane is not present. On the contrary, at the second stage ignition methane burns at higher temperature compared to diesel-only case. As the second micro-pilot starts at 5° ATDC, for non-methane case temperature suddenly drops as spray is being injected in the developed flame kernel of the first pilot injection. Start of the second micro-pilot is visible in Fig. 8.8. This effect is reduced in case of multi-pilot injection due to the presence of methane, and flame kernel grows with steady consumption of fuel. Split injection proves to be effective in controlling end-gas ignition and growth of the flame kernel. The current way of modeling proved to be very effective in detecting changes in the end-gas ignition temperature as well as its precise location and frequency.

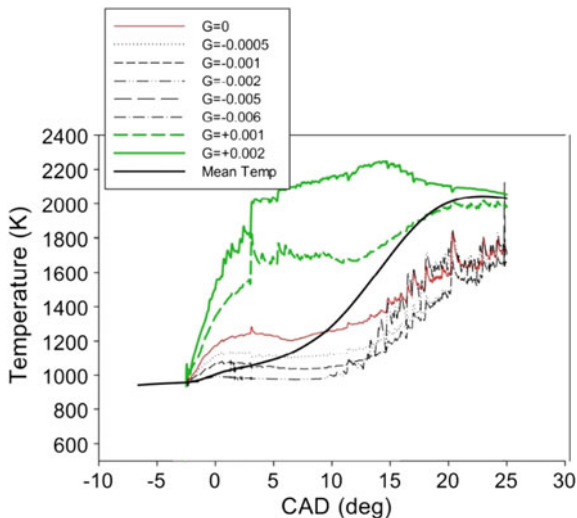


Fig. 8.11 Temperature profiles for different G values for the case with the first and second pilot injection. RPM—1000, P_{inj} —40 MPa, CH_4 —26.7 mg/cyl, diesel inj—first (6° BTDC)—0.8 mg/cyl, second (5° ATDC)—0.8 mg/cyl, λ —1.66, IMEP—0.82 MPa

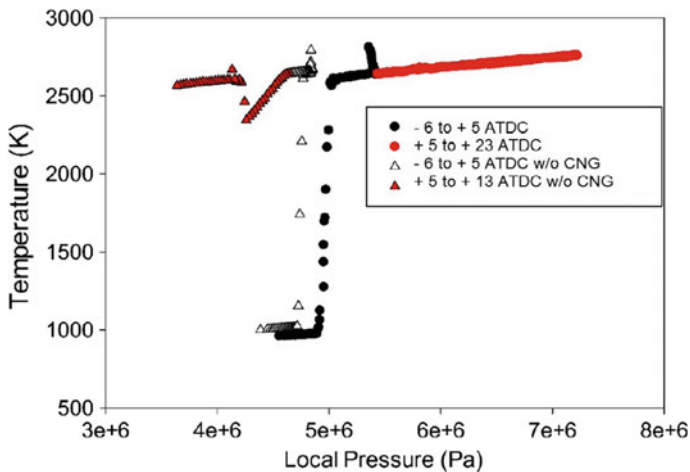


Fig. 8.12 Local temperature–pressure relationship for the case with the first and second pilot injection with and without methane/CNG

8.3 Combustion of Natural Gas in Homogeneous Charge Compression Ignition (HCCI) Engines

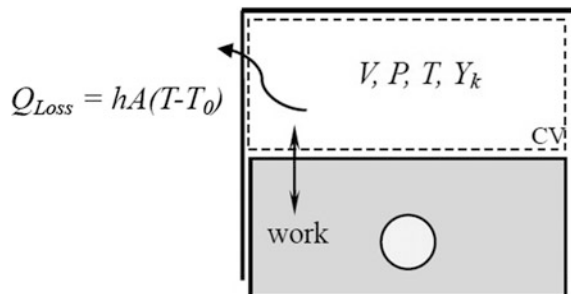
NG requires little time for mixture preparation and is chemically stable, both of which make it a suitable fuel for homogeneous charge compression ignition (HCCI) engines. NG produces less greenhouse gas emissions compared to those of petroleum-based fuels. NG also brings a few challenges for HCCI engine operations. NG has a high octane number and therefore is hard to auto-ignite. In addition, NG usually has large differences in fuel composition from field to field, which adds more uncertainties for engine applications to make universal adjustments to run on different NG types. To enable the use of NG in HCCI engines, higher compression ratios, significant amount of intake heating, some types of preignition and/or internal EGR are required to be adjusted to ensure the auto-ignition.

The use of NG in HCCI engines has been studied for over a decade. The obtained results (Ando et al. 2003; Jun et al. 2003) experimentally showed the effect of different operating parameters such as intake temperature, density, equivalence ratio, and others, on natural gas auto-ignition characteristics. Yap et al. (2004) experimentally demonstrated the decrease of NO_x emissions and increase of CO and UHC emissions with the addition of reformed EGR. The same group (Yap et al. 2006) also reported an increase in NO_x emissions with hydrogen addition at higher loads in a natural gas HCCI engine. Other groups (Doughty et al. 1992) investigated the effect of engine loads and measured the lower NO_x emissions in the exhaust gas at lower loads and at higher engine speeds.

8.3.1 Single-Zone Model

To simulate NG HCCI combustion in IC engines, a single-zone model with distinct chemical kinetics in CHEMKIN can be employed (CHEMKIN-PRO 2010). The fundamental assumption that the model imposes is that the temperature and species concentrations are viewed as homogeneous throughout the cylinder. The thermodynamic system described by the model is shown in Fig. 8.13. In the cylinder, there

Fig. 8.13 Piston–cylinder system schematics of the single-zone thermodynamic model



are four independent properties which include temperature (T), species concentration (Y_k), pressure (P), and volume (V). The heat is transferred to the cylinder wall, and the work is transferred by the piston. The main equations are described below.

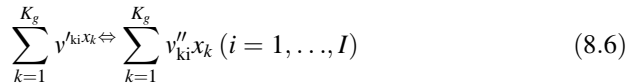
The species conservation for the system is (CHEMKIN-PRO 2010),

$$(\rho V) \frac{dY_k}{dt} = (\dot{\omega}_k V) W_k \quad (8.4)$$

where Y_k is the mass fraction, W_k is the molecular weight, ρ is the mass averaged density, and $\dot{\omega}_k$ is the molar rate of production per volume. The energy equation for the system shown in Fig. 8.13 is the following (CHEMKIN-PRO 2010),

$$\frac{dU}{dt} = -\dot{Q}_{\text{loss}} - P \frac{dV}{dt} \quad (8.5)$$

Elementary reactions involving K_g species can be represented in the general form,



where ν_{ki}^{\prime} and $\nu_{ki}^{\prime\prime}$ indicates forward and reverse stoichiometric coefficients for the i th reaction, and x_k is the chemical symbol of the k th species. Then, the expression for the production rate $\dot{\omega}_k$ can be obtained,

$$\dot{\omega}_k = \sum_{i=1}^I \left[(\nu_{ki}^{\prime\prime} - \nu_{ki}^{\prime}) \left(k_{fi} \prod_{k=1}^{K_g} [X_k]^{\nu_{ki}^{\prime}} - k_{ri} \prod_{k=1}^{K_g} [X_k]^{\nu_{ki}^{\prime\prime}} \right) \right] \quad (k = 1, \dots, K) \quad (8.7)$$

where k_{fi} and k_{ri} are the forward and reverse rate constants of the i th reactions, and $[X_k]$ is the molar concentration of the k th species. The forward rate constants for the reactions are generally the inputs of the model.

Arrhenius temperature dependence:

$$k_{fi} = A_i T^{\beta_i} \exp\left(-\frac{E_i}{R_c T}\right) \quad (8.8)$$

Instantaneous spatially averaged heat transfer to the cylinder wall is calculated using a version of the Woschni correlation (Heywood 1988). This version has been adjusted for HCCI combustion (CHEMKIN-PRO 2010), as shown below,

$$Nu_h = a \cdot Re^b \cdot Pr^c = 0.035 Re^{0.8} \quad (8.9)$$

where $a = 0.035$, $b = 0.8$, $c = 0$.

$$Re = \frac{\rho w B}{\mu} \tag{8.10}$$

where the local average gas velocity w is correlated as follows,

$$w = \left[\left(C_{11} + C_{12} \frac{v_{swirl}}{\bar{v}_p} \right) \bar{v}_p + C_2 \frac{V_d T_r}{p_r V_r} (p - p_m) \right] \tag{8.11}$$

where V_d is the displaced volume; p is the instantaneous cylinder pressure; p_r , V_r , T_r are the pressure, volume, and temperature at the reference state; p_m is the motored cylinder pressure at the same crank angle as p . In this study, $C_{11} = 2.28$, $C_{12} = 0.308$, $C_2 = 0.54$, and $v_{swirl} = 0$ are used. More detailed description of this heat transfer correlation can be found in (Heywood 1988).

8.3.2 Multi-zone Model

Multi-zone models typically require non-reacting (cold flow) fluid mechanics simulation to provide the initial temperature and concentration distributions in the cylinder. With these initial distributions, an appropriate number of zones can be determined and those zones can be established and initialized with different temperatures and concentrations. Figure 8.14 shows an example of the setup procedure where the continuous temperature distribution from the CFD simulation is converted to the zonal conditions in the multi-zone model. After the zonal initial

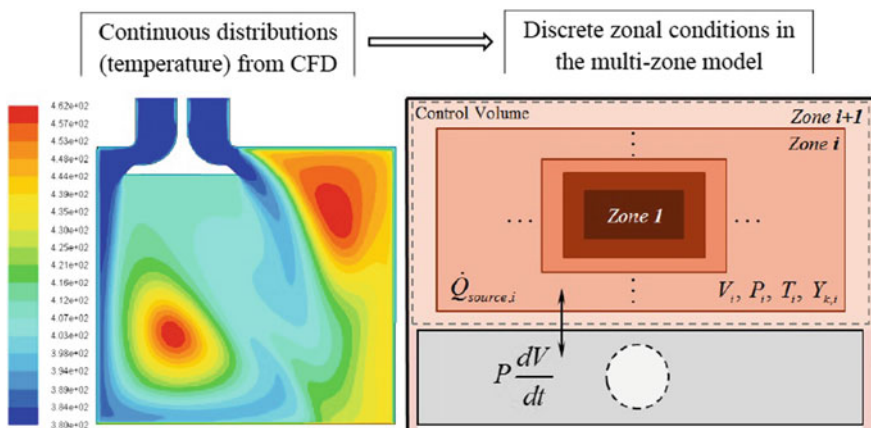


Fig. 8.14 Illustration of the multi-zone model setup procedure, temperature distribution from CFD (left) and zonal conditions in multi-zone model (right) (CHEMKIN-PRO 2010)

conditions are set up, the detailed chemical kinetics can be applied and solved in all zones fully coupled.

The assumptions (CHEMKIN-PRO 2010) pertaining to this model formulation are as follows. First of all, all zones are assumed to have the same, uniform pressure. Second, the mass or heat transfer between zones is assumed to be negligible and the only interaction between the zones is the compression work. Third, the total volume of the zones must equal the cylinder volume computed by the slider-crank relationship used in the single-zone internal combustion engine model. This constraint is used to determine the zonal and cylinder pressure (CHEMKIN-PRO 2010).

The governing equations for the multi-zone model are similar to those for the single-zone model, except for the additional superscript “*i*” which represent the zone number, as shown in Eq. 8.12 (conservation of species) and Eq. 8.13 (energy equation) (CHEMKIN-PRO 2010).

$$(\rho^i V^i) \frac{dY_k^i}{dt} = (\dot{\omega}_k^i V^i) W_k^i \quad \text{for } i = 1, 2, \dots, N \text{ zones} \quad (8.12)$$

$$(\rho^i V^i) c_p^{-i} \frac{dT^i}{dt} = -V^i \sum_{k=1}^{K_g} (h_k^i \dot{\omega}_k^i) W_k^i + V^i \frac{dP}{dt} - \dot{Q}_{\text{loss}}^i \quad \text{for } i = 1, 2, \dots, N \text{ zones} \quad (8.13)$$

The single-zone and multi-zone models have been validated against the experimental work done by Jun et al. (2003). The operating conditions at which the prediction and measurements were compared are summarized in Table 8.3. The temperatures at intake valve closure (IVC) are used to calibrate the start of combustion for both the single-zone and multi-zone simulations. Figures 8.15 and 8.16

Table 8.3 Initial conditions for the 0D simulation and the experiments from (Jun et al. 2003)

Parameters	Single- and multi-zone models	Experiment by Jun et al. (2003)
Engine speed (RPM)	800	800
IVC timing	-132 ATDC	-132 ATDC
Intake manifold temperature (K)	N/A	380
Intake manifold pressure (K)	N/A	1.6
Temperature at IVC (K)	417	N/A
Pressure at IVC (bar)	1.6	N/A
Wall temperature (K)	450	N/A
Equivalence ratio	0.2–0.45	0.2–0.45
Natural gas composition (mole fraction)	CH ₄ —88%, C ₂ H ₆ —6%, C ₃ H ₈ —4%, C ₄ H ₁₀ —2%	CH ₄ —88%, C ₂ H ₆ —6%, C ₃ H ₈ —4%, C ₄ H ₁₀ —2%

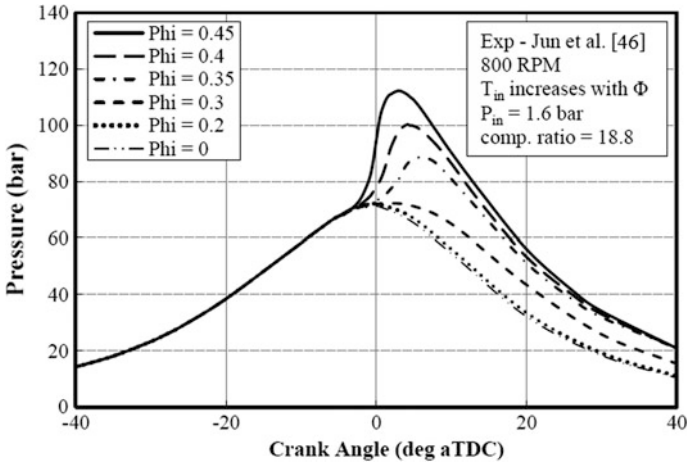


Fig. 8.15 In-cylinder pressure as a function of crank angle (Zheng and Caton 2012)

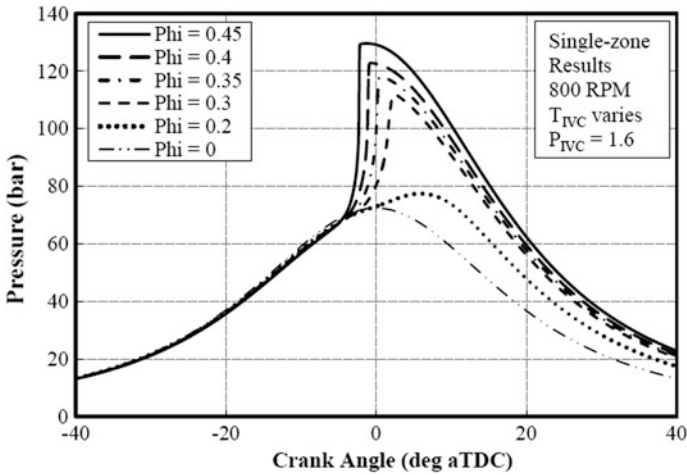


Fig. 8.16 In-cylinder pressure predicted as a function of crank angle (Zheng and Caton 2012)

show the measured and predicted pressure traces as a function of crank angle at various equivalence ratios. The results for multi-zone analysis have generally better agreement with the measurements than single-zone simulations and are provided in reference (Zheng 2012).

8.3.3 Engine Efficiencies for Using Natural Gas in Comparison with Gasoline

This section continues to compare natural gas with gasoline in terms of the indicated efficiency and volumetric efficiency at the best efficiency point under various operating conditions. Some of the fuel properties are shown in Table 8.4.

For all of the equivalence ratios presented here, about 3% difference in indicated efficiencies is observed between the two fuels. The efficiencies for the natural gas cases are lower largely due to the higher heat loss and lower specific heat ratio. Higher heat transfer is a direct result of higher combustion temperature. Lower specific heat ratio is caused by the higher mole fraction of the fuel species since natural gas has much lower molar stoichiometric air–fuel ratio than gasoline. A reduction of specific heat ratio reduces the amount of energy that can be extracted by the piston. At very low equivalence ratio, the chemical kinetics and combustion become slower and less complete which affects the thermal efficiency.

As the equivalence ratio increases, though combustion efficiency is improved, the heat loss as well as the fraction of heat loss out of total fuel energy is greater as a result of a higher combustion temperature. In addition, higher equivalence ratio leads to lower specific heat ratio which reduces the thermal efficiency. So the indicated efficiency reaches a peak around ϕ equal to 0.3. In terms of the volumetric efficiency, it is straightforward that the gasoline cases are higher and the differences are larger at higher equivalence ratios, since volumetric efficiency is strongly affected by the intake temperature. This observation poses another issue for using natural gas in HCCI engines which is the relatively lower torque output at the same equivalence ratio due to the low volumetric efficiency (Zheng 2012).

The indicated thermal efficiency for both natural gas and gasoline increases as the engine speed increases. This increase is again related to the amount of heat transfer. Although the temperature at the IVC is higher at higher speeds, less time is allowed for transferring heat from the gas to the walls as the real time of one cycle becomes shorter as engine speed increases. The overall effect is to reduce the fraction of heat loss out of total fuel energy and to improve the thermal efficiency. The volumetric efficiency, however, decreases with the increase of engine speeds. Again, this is directly dictated by the higher IVC temperature at higher speeds. So running HCCI engines, either with gasoline or natural gas, at higher speeds could improve thermal efficiency but at the penalty of torque output (Zheng 2012).

Table 8.4 Fuel properties of natural gas and gasoline

Fuel surrogate	Lower heating value (kJ/kmol)	Lower heating value (kJ/kg)	Stoichiometric A/F ratio, molar	Stoichiometric A/F ratio, mass	Adiabatic flame temperature (K)
Natural gas	9.35×10^5	49,626	10.98	16.79	2596
Gasoline	4.71×10^6	43,927	54.95	14.78	2636

The indicated thermal efficiency approximately remains nearly constant as the EGR level changes for both natural gas and gasoline cases. This might be attributed to the balance between lowered combustion temperature due to the EGR dilution effect and increased IVC temperature. Volumetric efficiency slightly drops as the EGR fraction increases and IVC temperature at best efficiency increases.

Having higher intake pressure slightly increases the indicated efficiency as a result of lower IVC temperature and corresponding lower heat loss. Furthermore, increasing intake pressure greatly improves the volumetric efficiency due to the increase in the mass of air–fuel mixture. These results imply that intake boosting is an attractive option to have for HCCI engines fueled with natural gas or other high octane fuels (Zheng 2012).

Using the single-zone model, Zheng (2012) conducted the analysis on the effect of operating conditions on the ignition characteristics, engine performance, and thermal efficiency of the HCCI engine. He found that the operating conditions, including equivalence ratio, engine speed, and intake pressure, have great influences on the HCCI ignition characteristics. The minimum required temperature at IVC for auto-ignition and complete combustion decreases as the equivalence ratio increases and the intake pressure increases, and increases as the engine speed increases. In addition to the operating conditions, compression ratio has an even greater effect on the minimum required temperature at IVC. For the natural gas case, the increase in compression ratio from 18 to 22 could reduce the requirement of the minimum required temperature at IVC by 40 K. The results imply that to reduce the intake temperature requirement for using natural gas, higher compression ratio, intake boosting, and relative lower engine speed are desirable.

The operating conditions have a great effect on the HCCI engine performance and efficiencies. The volumetric efficiency increases with the increase of equivalence ratio or intake pressure or the decrease of engine speed or exhaust gas recirculation level. The indicated thermal efficiency peaks at a certain equivalence ratio, and a higher or lower equivalence ratio than this value will decrease the indicated efficiency. The increase in engine speed improves the indicated efficiency, while the change in intake pressure and EGR level does not have a strong influence on the efficiency. In terms of the volumetric efficiency, intake boosting is a very desirable option to increase the specific power output, and operating at high engine speed is not attractive as it deteriorates the volumetric efficiency. In terms of the indicated efficiency, operating with a relatively lean mixture is still a desirable option for natural gas HCCI engines.

8.4 Combustion of Natural Gas in Reactivity Controlled Compression Ignition (RCCI) Engines

Reactivity controlled compression ignition (RCCI) concept can significantly improve the combustion process in terms of efficiency and exhaust gas emissions (Reitz and Duraisamy 2015). Recent interest has been raised to investigate RCCI combustion concept with NG/diesel fuels at different engine operating conditions (Ansari et al. 2016; Nieman et al. 2012; Zoldak et al. 2014, 2015; Doosje et al. 2014; Xu et al. 2016).

8.4.1 Effect of Energy-Based Premixed Ratio

Figure 8.17 shows the effect of premixed ratio (PR) on heat release rate (HRR) and in-cylinder pressure. The NG premixed ratios were composed to provide the same amount of the total energy for combustion. The graph shows that sweeping the PR from 55 to 95% increases the ignition delay and reduces the in-cylinder pressure and HRR (Poorghasemi et al. 2017).

Figure 8.18 shows that when the pressure ratio increases, the in-cylinder temperature decreases. This can result in the increase of HC emissions. It can also be explained by the fact that the crevice regions near the walls are usually colder in higher-pressure ratios. This will lower the combustion efficiency and increase the UHC emissions.

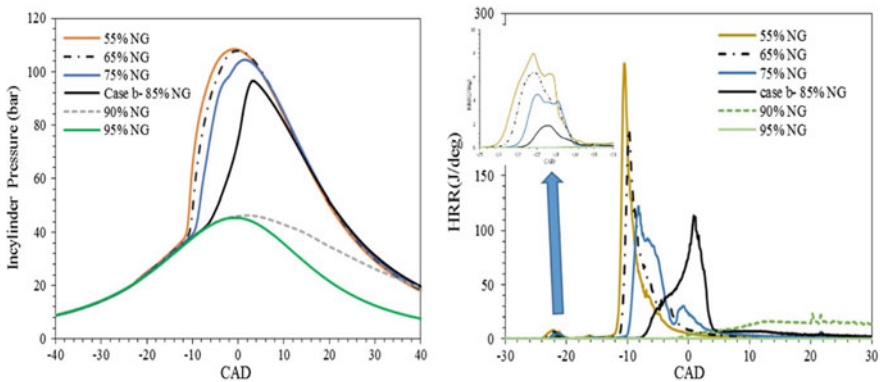


Fig. 8.17 Effects of PR of in-cylinder mixture on in-cylinder pressure (left) and HRR (right) (Poorghasemi et al. 2017)

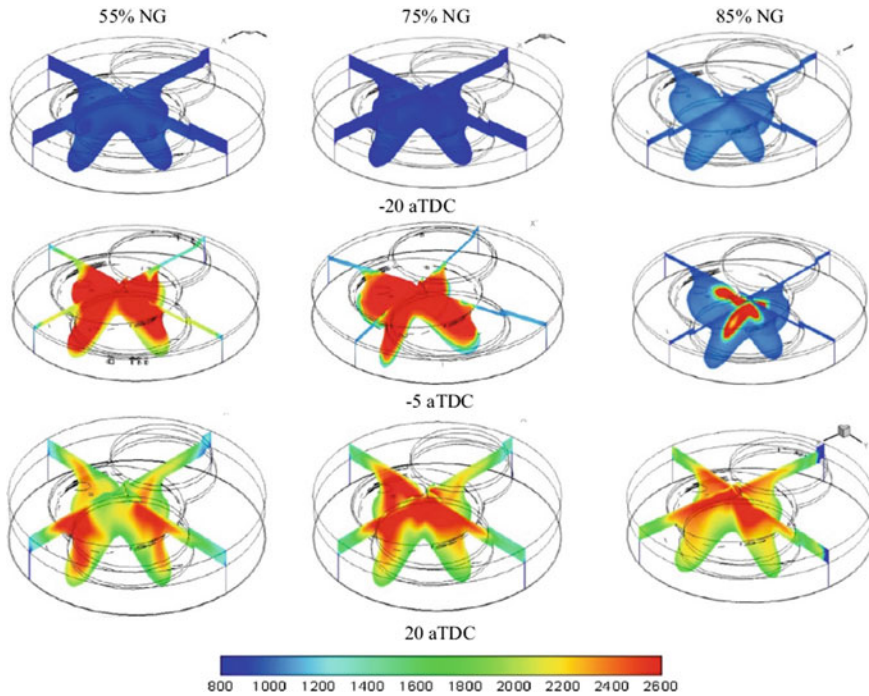


Fig. 8.18 Effects of PR on in-cylinder temperature (Poorghasemi et al. 2017)

8.4.2 Effect of Injection Timing

The first injection timing

The effect of the first injection timing (SOI1) was once completed by changing SOI1 from 85° to 45° BTDC while maintaining SOI2 timing consistent at 20° BTDC. Seventy percentage of the total diesel fuel was injected at the first pulse and 30% at the second pulse. Advancing SOI1 timing from 85° to 45° BTDC results in delayed combustion and reduced peak in-cylinder pressure and HRR, as shown in Fig. 8.19. This happened due to the increase of the mixing time and better homogeneity of NG and diesel fuel, and as a result, less reactive mixture was prepared (Curran et al. 2012; Ma et al. 2013).

As the SOI1 timing is retarded, NO_x emission increases and HC and CO emissions decrease. NO_x increases due to the increase of the in-cylinder temperature. As shown in Fig. 8.20, the spray is impinged on the wall and enters the crevice cavity where due to the established lower temperature and lower volume to surface ratio zones HC and CO emissions increase. In later SOI1 at 45° BTDC, a greater

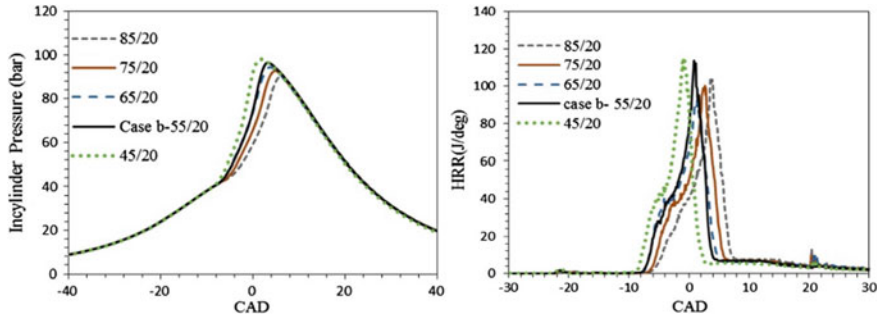


Fig. 8.19 Effects of SOI1 timing on in-cylinder pressure (left) and HRR (right) for the engine operating condition (Poorghasemi et al. 2017)

amount of fuel is injected into the areas of piston bowl and squish areas with higher temperature and reactivity gradients, and consequently, lower levels of HC and CO produced.

The second injection timing

The second fuel injection timing (SOI2) was changed from 40° to 0° BTDC, with constant SOI1 timing at 55° BTDC, as shown in Fig. 8.21. The results showed that retarding the SOI2 from 40° to 0° BTDC caused the retard of the combustion phasing, which caused the peak of in-cylinder pressure to be decreased. The second diesel injection pulse could not mix properly with in-cylinder mixture due to a very short time period, and this has caused the ignition delay to be increased.

Figure 8.22 shows the effect of SOI2 sweep on in-cylinder temperature. The simulation results showed that high local in-cylinder temperature region near TDC occurred that has caused the NO_x to be increased at earlier SOI2 timings. When SOI2 was advanced, the lowest carbon monoxide and unburnt hydrocarbon emissions were achieved. When the injection SOI2 was initiated at 40° BTDC, the flame could reach the whole combustion chamber, while at SOI2 at 0° BTDC there are more regions with lower temperatures, as shown in Fig. 8.22. This causes a lower combustion efficiency and higher levels of unburnt hydrocarbons and carbon monoxide emissions at later SOI2 timings (Paykani et al. 2015).

8.5 Advanced Ignition Systems for Natural Gas Combustion

Due to high octane number, natural gas engines can be operated at relatively higher compression ratios and leaner fuel–air mixtures, thus leading to higher thermal efficiencies and lower emissions. However, this can lead to considerable reduction in power density. This can be compensated by increasing the pressure of combustible charge at the end of a compression stroke. To ignite a leaner air–fuel charge

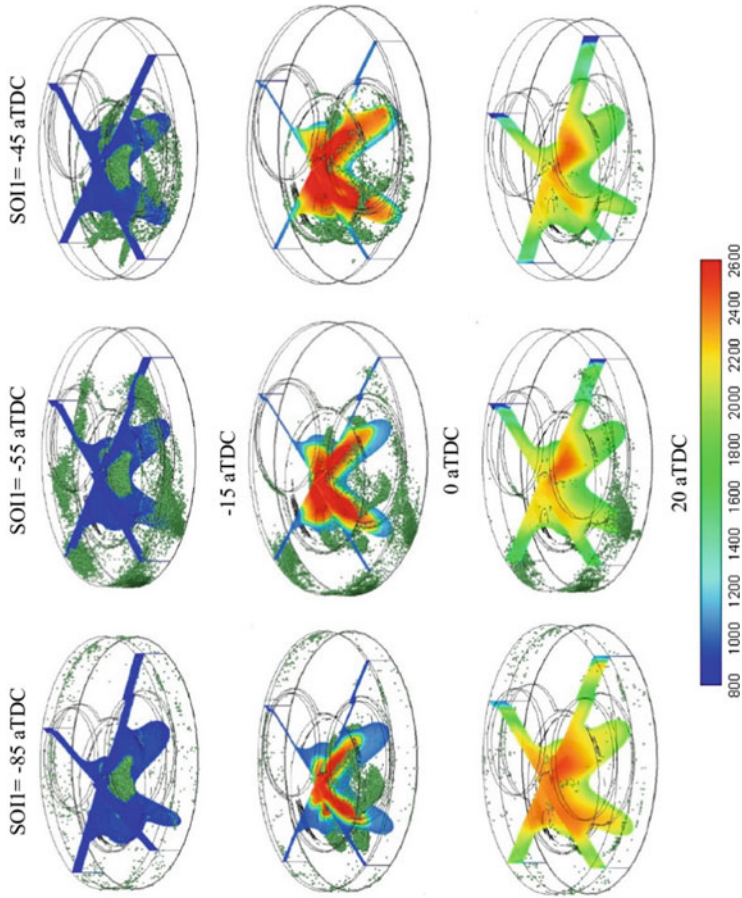


Fig. 8.20 Effects of SOI on in-cylinder temperature for the engine operating condition (Poorghasemi et al. 2017)

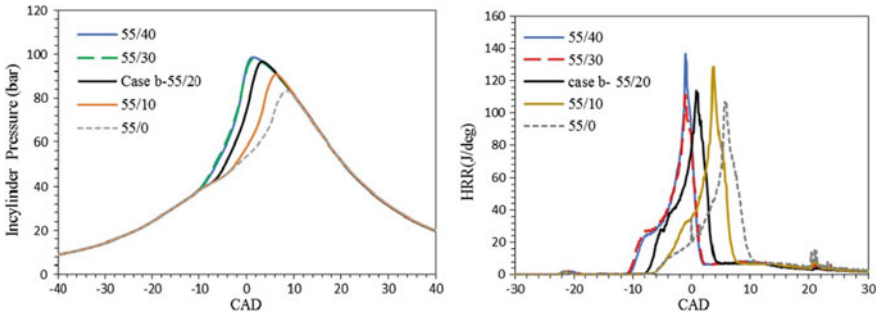


Fig. 8.21 In-cylinder pressure (left) and HRR (right) versus SOI2 timing (Poorghasemi et al. 2017)

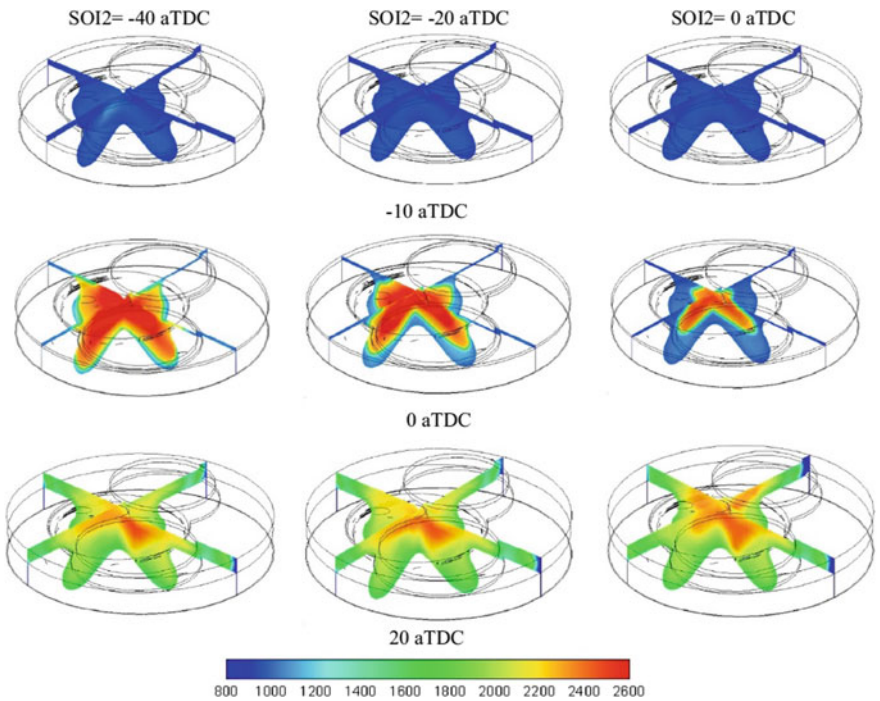


Fig. 8.22 Effects of SOI2 on in-cylinder temperature (Poorghasemi et al. 2017)

at higher pressures requires using much higher voltage ignition systems. These high voltages significantly reduce the lifetime of spark plugs (Wienrotter et al. 2006). Such ignition systems are a laser-assisted ignition and a plasma-assisted ignition, which are discussed below.

8.5.1 Laser-Assisted Ignition Control

Laser can be used as an alternative ignition source for engines. Laser pulses delivered with the aid of a laser system are targeted inside the combustion chamber with fuel–air mixture. The experimental laser ignition system was designed and constructed by Srivastava et al. (2011) and is shown in Fig. 8.23.

The obtained high-speed camera images that display the development of the early flame kernel stages with time had been recorded using shadowgraphy technique. The images were obtained at 54,000 fps. The snapshots were captured at an interval of 18.5 ms for a combustion event. From these images, we can get an idea on how the flame kernel is developed with time for selected NG–air ratios ($\lambda = 1.2$ and $\lambda = 1.6$). Figure 8.24 shows the sequential snapshots of flame kernel development at unique timescales for $\lambda = 1.2$. Timescales of the first four snapshots were kept constant; however, the timescales for the final four snapshots were different due to the fact of longer combustion duration for the leaner mixtures. The vertical and horizontal dimensions of all images have been kept constant at 1.15 and 1.45 cm, respectively.

Srivastava et al. (2011) found that the flame kernel propagation distance was consistently decreasing with leaner mixtures $\lambda = 1.6$, as shown in Fig. 8.25. These findings suggest that the volumetric growth of the flame kernel reduces substantially with the reduction of NG–air mixture strength and a practical laser ignition system applied to the engine will not be able to deal with NG–air mixtures leaner than $\lambda = 1.6$.

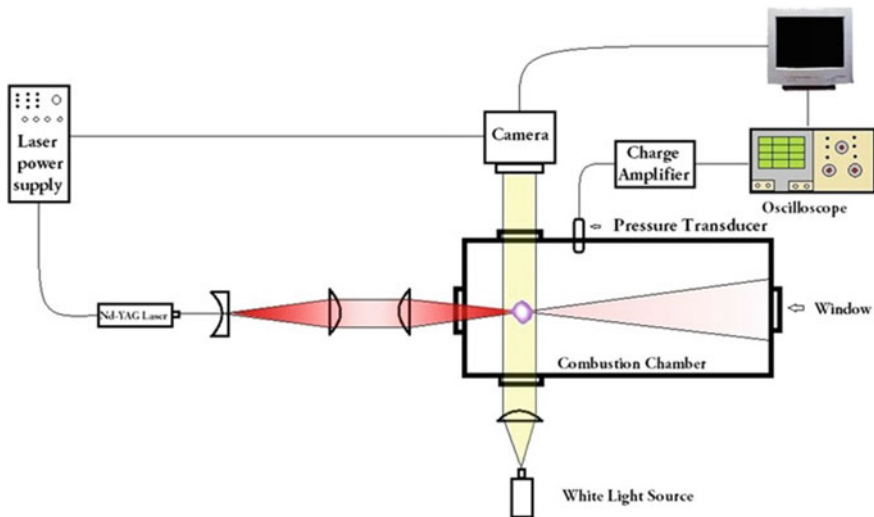


Fig. 8.23 Schematic diagram of laser ignition shadowgraphy of NG–air mixture (Srivastava et al. 2011)

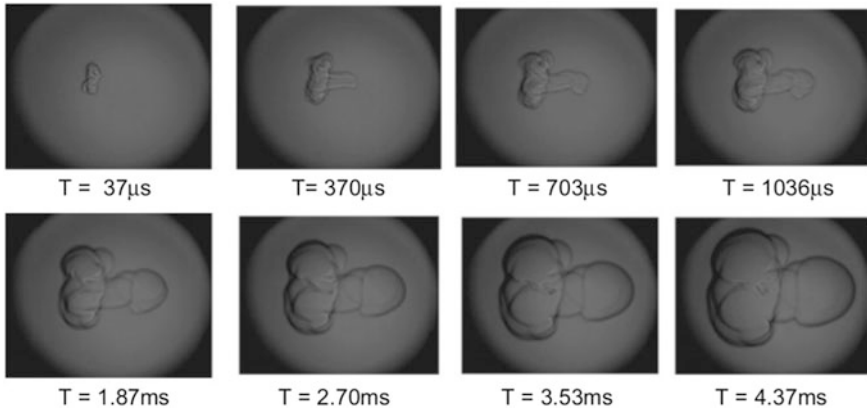


Fig. 8.24 Shadowgraph image of flame kernel development ($\lambda = 1.2$) (Srivastava et al. 2011)

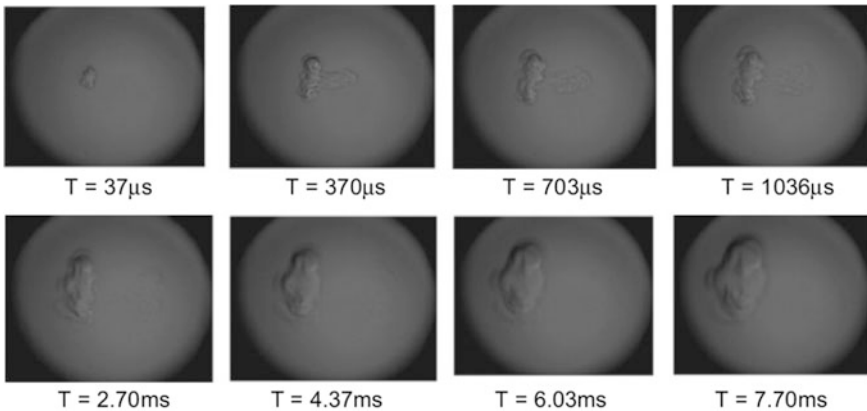


Fig. 8.25 Shadowgraph image of flame kernel development ($\lambda = 1.6$) (Srivastava et al. 2011)

To observe the laser ignition process under the reciprocating engine conditions, Dumitrache et al. (2017) used rapid compression machine (RCM) shown in Fig. 8.26. Details of this setup are given in the reference (Dumitrache et al. 2017).

The approach validated in this study used to be for a laser-ignited mixture of CH_4 -air at an equivalence ratio of $= 0.5$ (Dumitrache et al. 2017), as shown in Fig. 8.27. The lean condition used to be chosen to restrain the flame propagation speed, hence allowing capturing numerous frames of the flame propagation, given the limitations of the imaging system. In these experiments, only 30% of the mixture has been consumed by the propagating flame and the chemical heat release overcomes the heat losses to the wall that causes the flame to become turbulent with cellular structure as shown in Fig. 8.27.

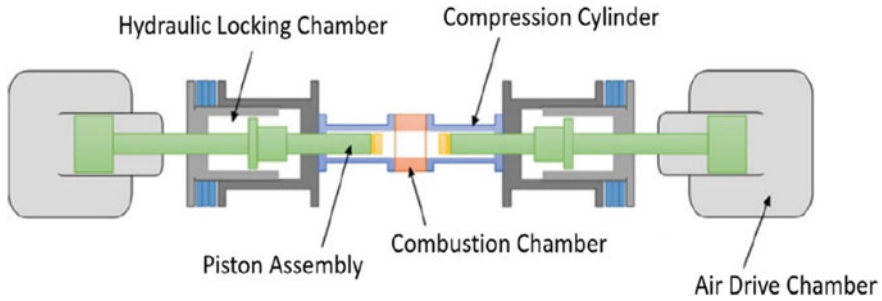


Fig. 8.26 Schematic drawing depicting the main components of the RCM (Dumitrache et al. 2017)

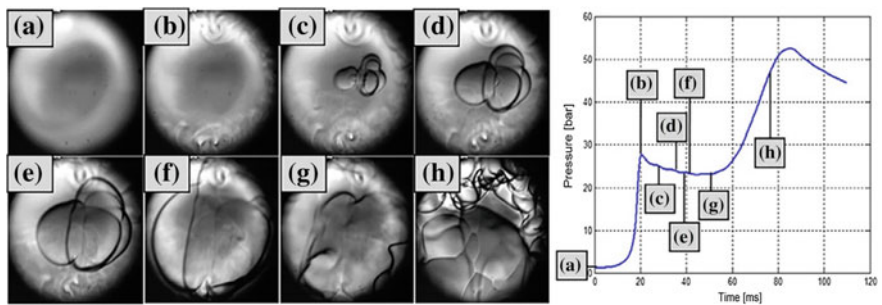


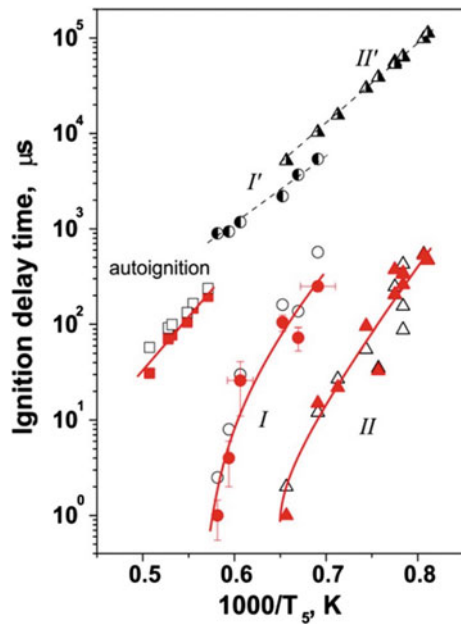
Fig. 8.27 Schlieren high-speed photography images of a laser-ignited CH_4 -air mixture ($\phi = 0.5$) inside the RCM. The images show the flame development and spread. The pressure trace shown at the right is used to correlate the frames with the actual RCM firing. The field of view is 20 mm (Dumitrache et al. 2017)

8.5.2 Plasma-Assisted Ignition and Combustion Control

In latest years, the plasma-assisted combustion mechanisms have been validated through experimentation under controlled conditions and by the way of evaluating the effects with numerical simulations of discharge and combustion processes. Researchers became curious about non-equilibrium plasma for ignition and combustion control (Starikovskii 2005, 2006) thanks to the new potentialities for ignition and flame stabilization that are supplied by the plasma-assisted approach. The most important distinction between the traditional combustion and plasma-assisted combustion is the ignition initiation mechanism.

Kosarev et al. (2008) and Aleksandrov et al. (2009) have observed a correlation between the ignition delay time and the temperature for the $\text{CH}_4/\text{O}_2/\text{Ar}$ mixture. The fuel discharge causes a drastic reduction in the ignition delay time and allows the mixture to ignite at notably lower temperatures. Figure 8.28 shows the ignition delay time in a $\text{CH}_4/\text{O}_2/\text{Ar} = 3.3:6.7:90$ mixture as a function of temperature for

Fig. 8.28 Ignition delay time in a $\text{CH}_4/\text{O}_2/\text{Ar} = 3.3:6.7:90$ mixture as a function of temperature for auto-ignition and ignition (I–II) with the plasma discharge. The closed and open symbols correspond to measurements and calculations, respectively, and the solid curves correspond to experimental data. The dashed lines I' and II' and the semi-closed symbols correspond to the calculations of the auto-ignition delay times as those in regions I and II (Kosarev et al. 2008; Aleksandrov et al. 2009)



auto-ignition and (I–II) ignition with the plasma discharge. The diagram indicates the comparison of the measured ignition delay time with and without plasma at the equal initial gas densities. As viewed in Fig. 8.28, these times may vary by two or three orders of magnitude.

Michael et al. (2010) showed that the ignition in CH_4 –air mixtures can be performed using low energy seed laser pulses and an overlapping subcritical microwave pulse. Very susceptible ionization by a laser localized the deposition of microwave energy and caused fast heating, high temperatures, and ignition. The same research team (Michael et al. 2010) also developed a coupled one-dimensional gas-dynamic/plasma-dynamic model to follow the rapidly evolving plasma and gas properties carried out through this interaction. By growing the pulse power by a factor of 3, the ignition used to be discovered alongside the seed laser path. In this case, a much larger area of strong coupling with the microwave (MW) energy was discovered in the shadowgraph snapshots as shown in Fig. 8.29 (Michael et al. 2010). For a large number of combustion-driven engines, transient plasma ignition involving quick ignition pulses (typically 10–50 ns) has been shown to efficiently minimize ignition delays and enhance engine performance compared to the conventional spark ignition.

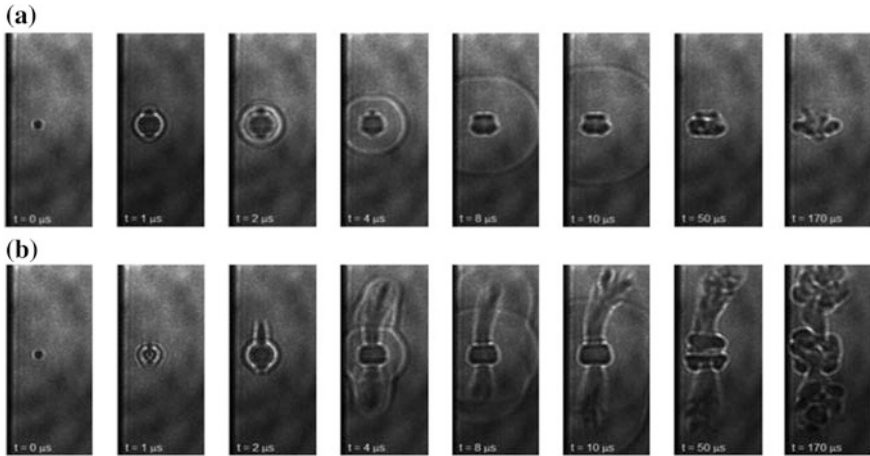


Fig. 8.29 Laser pulse–MW evolution in air. **a** Laser spot evolution. **b** Laser + MW evolution (Michael et al. 2010)

8.6 Conclusion

The chapter summarizes the advanced combustion and ignition technologies with natural gas as a fuel for application in internal combustion engines. Natural gas is considered the direct alternative to replace the crude oil-derived liquid fuels for better energy efficiency and cleaner environment. It was demonstrated by several researchers that the novel combustion technologies such as PREMIER, HCCI, and RCCI can provide better fuel efficiency and emission reduction. However, these technologies should be further developed to become applicable and feasible to a wider range of engine design and operating conditions with natural gas.

These technologies will become even more useful during the transport electrification era. With the requirements to introduce more electric vehicles in transportation network, more challenges will appear to meet required power and mileage levels, especially for commercial heavy-duty vehicles and trucks. The analysis shows that in the near future it will not be possible to convert the entire heavy-duty vehicles fleet to run on electric batteries only, and therefore, the hybrid powertrain systems will have to be used to ensure the cost-effective and reliable operation. In this situation, hybrid powertrain systems with natural gas as a fuel for internal combustion engines will become a feasible solution.

Along with the novel combustion technologies for effective burning of fuel inside the engine cylinders, more advanced ignition initiation technologies are also being developed and applied to conventional and future internal combustion engines. Such technologies are laser-assisted and plasma-assisted ignition systems. Lasers are becoming feasible candidates as alternative ignition systems in internal combustion engines. This technology can be applied to initiate the combustion of high octane number natural gas mixtures. Plasma formation does not always

imply that ignition has to take place. Only if the energy content of the plasma is excessive enough, then the mixture of NG–air is ignited by a flame kernel, which may also extend or extinguish. This plasma source can be applied as a stand-alone or additional source to initiate the combustion in internal combustion engines.

Natural gas can play an important role as an actual game changer in energy and transport sectors for energy security. For the consumer’s perspectives to make a swap from current liquid fuels to compressed natural gas will be more compelling than for other alternatives such as ethanol or electricity.

References

- Agarwal AK, Singh AP, Maurya RK (2017) Evolution, challenges and path forward for low temperature combustion engines. *Prog Energy Combust Sci* 61(7):1–56
- Aleksandrov NL, Kindysheva SV, Kosarev IN, Starikovskaia SM, Starikovskii AY (2009) Mechanism of ignition by nonequilibrium plasma. *Proc Combust Inst* 32:205–212
- Ando T, Isobe Y, Sunohara D, Daisho Y, Kusaka J (2003) *JSAE Rev* 24:33–40
- Ansari E, Poorghasemi K, Irdmousa BK, Shahbakhti M, Naber J (2016) Efficiency and emissions mapping of a light duty diesel-natural gas engine operating in conventional diesel and RCCI modes. In: SAE international powertrain, fuel and lubricants conference, 2016-01-2309
- Aoyama T, Hattori Y, Mizuta J, Sato Y (1996) An experimental study on premixed charge compression ignition gasoline engine. SAE technical paper SAE960081
- Asad U, Divekar P, Zheng M, Tjong J (2013) Low temperature combustion strategies for compression ignition engines: operability limits and challenges. SAE 2013-01-0283
- Azimov U, Tomita E, Kawahara N, Harada Y (2011) Premixed mixture ignition in the end-gas region (PREMIER) combustion in a natural gas dual-fuel engine: operating range and exhaust emissions. *Int J Engine Res* 12:484–497
- Benajes J, Molina S, Garcia A, Monsalve-Serrano J (2015) Effects of low reactivity fuel characteristics and blending ratio on low load RCCI performance and emissions in a heavy-duty diesel engine. *Energy* 90:1261–1271
- Caton J (2011) Thermodynamic advantages of low temperature combustion (LTC) engines using low heat rejection (LHR) concepts. SAE 2011-01-0312
- CHEMKIN-PRO Theory Manual, 2010
- Christensen M, Johansson B (1998) Influence of mixture quality on homogeneous charge compression ignition. SAE technical paper 982454
- Curran S, Hanson R, Wagner R (2012) Reactivity controlled compression ignition combustion on a multi cylinder light-duty diesel engine. *Int J Engine Res* 13(3):216–225
- Dempsey A, Walker N, Gingrich E, Reitz R (2014) Comparison of low temperature combustion strategies for advanced compression ignition engines with a focus on controllability. *Combust Sci Technol* 186(2):210–241
- Doosje E, Willems F, Baert R (2014) Experimental demonstration of RCCI in heavy duty engines using diesel and natural gas. SAE 2014-01-1318
- Doughty GE, Bell SR, Midkiff KC (1992) *J Eng Gas Turbines Power* 114:459–465
- Dumitrache C, Baumgardner M, Boissiere A, Maria A, Roucis J, Marchese AJ, Yalin A (2017) A study of laser induced ignition of methane–air mixtures inside a rapid compression machine. *Proc Combust Inst* 36:3431–3439
- El Merhubi H, Keromnes A, Catalano G, Lefort B et al (2016) A high pressure experimental and numerical study of methane ignition. *Fuel* 177:164–172

- Gharehghani A, Hosseini R, Mirsalim M, Jazayeri A, Yusaf T (2015) An experimental study on reactivity controlled compression ignition engine fueled with biodiesel/natural gas. *Energy* 89:558–567
- Gharehghani A, Mirsalim M, Jazayeri A (2016) Experimental study on low temperature combustion dual fuel biodiesel/natural gas engine. ASME technical paper 1:V001T03A001
- Gulder OL (1984) Correlations of laminar combustion data for alternative S.I. engine fuels. SAE technical paper 841000
- Heywood JB (1988) *Internal combustion engine fundamentals*. McGraw-Hill Book Company, New York
- Hosmath RS, Banapurmath NR, Khandal SV et al (2016) Effect of compression ratio, CNG flow rate and injection timing on the performance of dual fuel engine operated on Honge oil methyl ester (HOME) and compressed natural gas (CNG). *Renewable Energy* 93(8):579–590
- Intenan S et al (2014) Impact of low temperature combustion attaining strategies on diesel engine emissions for diesel and biodiesels: a review. *Energy Convers Manage* 80:329–356
- Jia M, Xie M, Wang T, Peng Z (2011) The effect of injection timing and intake valve close timing on performance and emissions of diesel PCCI engine with a full engine cycle CFD simulation. *Appl Energy* 88(9):2967–2975
- Jun D, Ishii K, Lida N. Combustion analysis of natural gas in a four stroke HCCI engine using experiment and elementary reactions calculation. SAE paper no. 2003-01-1089
- Kakae A, Rahnama P, Paykani A (2015) Influence of fuel composition on combustion and emissions characteristics of natural gas/diesel RCCI engine. *J Nat Gas Sci Eng* 25:58–65
- Kokjohn S, Hanson R, Splitter D, Reitz R (2010) Experiments and modeling of dual fuel HCCI and PCCI combustion using in-cylinder fuel blending. *SAE Int J Eng* 2(2):24–39
- Kokjohn S, Hanson R, Splitter D, Reitz R (2011) Fuel reactivity controlled compression ignition (RCCI): a pathway to controlled high-efficiency clean combustion. *Int J Eng Res* 12:209–226
- Kosarev IN, Aleksandrov NL, Kindysheva SV, Starikovskaia SM, Starikovskii AYU (2008) Kinetics of ignition of saturated hydrocarbons by nonequilibrium plasma: CH₄-containing mixtures. *Combustion and Flame* 154:569–586
- Laguitton O, Crua C, Cowell T, Heikal M, Gold M (2007) The effect of compression ratio on exhaust emissions from a PCCI diesel engine. *Energy Convers Manage* 48(11):2918–2924
- Li J, Yang W, Ana H, Zhao D (2015a) Effects of fuel ratio and injection timing on gasoline/biodiesel fueled RCCI engine: a modeling study. *Appl Energy* 155:59–67
- Li J, Yang W, An H, Zhou D, Yu W, Wang J et al (2015b) Numerical investigation on the effect of reactivity gradient in an RCCI engine fueled with gasoline and diesel. *Energy Convers Manage* 92:342–352
- Liang L, Reitz RD, Iyer CO, Yi J (2007) Modeling knock in spark-ignition engines using a G-equation combustion model incorporating detailed chemical kinetics. SAE technical paper 2007-01-0165
- Long L (2006) *Multidimensional modeling of combustion and knock in spark-ignition engines with detailed chemical kinetics*. University of Wisconsin-Madison
- Ma SH, Zheng Z, Liu H, Zhang Q, Yao M (2013) Experimental investigation of the effects of diesel injection strategy on gasoline/diesel dual-fuel combustion. *Appl Energy* 109:202–212
- Michael JB, Dogariu A, Shneider MN, Miles RB (2010) Subcritical microwave coupling to femtosecond and picosecond laser ionization for localized, multipoint ignition of methane/air mixtures. *J Appl Phys* 108(9) (Nov 1 2010)
- Molina S, Garcia A, Pastor J, Belarte E, Balloul I (2015) Operating range extension of RCCI combustion concept from low to full load in a heavy-duty engine. *Appl Energy* 143:211–227
- Musculus Mark PB, Miles Paul C, Pickett Lyle M (2013) Conceptual models for partially premixed low temperature diesel combustion. *Prog Energy Combust Sci* 39(2–3):246–283
- Nieman D, Dempsey A, Reitz RD (2012) Heavy-duty RCCI operation using natural gas and diesel. *SAE Int J Eng* 5(2):270–285
- Paykani A, Kakae A, Rahnama P, Reitz R (2015) Effects of diesel injection strategy on natural gas/diesel reactivity controlled compression ignition combustion. *Energy* 90:814–826

- Peters N (2000) *Turbulent Combustion*. Cambridge University Press, Cambridge, ISBN 9780521660822
- Pitsch BH (2002) A *G*-equation formulation for large-eddy simulation of premixed turbulent combustion. *Cent Turbul Res Annu* 4–7
- Poorghasemi K, Khoshbakhti Saray R, Ansari E, Khoshbakht Irdmousa B, Shahbakhti M, Naber JD (2017) Effect of diesel injection strategies on natural gas/diesel RCCI combustion characteristics in a light duty diesel engine. *Appl Energy* 199:430–446
- Reitz R (2013) Directions in internal combustion engine research. *Combust Flame* 160:1–8
- Reitz RD, Duraisamy G (2015) Review of high efficiency and clean reactivity controlled compression ignition (RCCI) combustion in internal combustion engines. *Prog Energy Combust Sci* 46:12–71
- Roy MM, Tomita E, Kawahara N, Harada Y, Sakane A (2009) Effect of fuel injection parameters on engine performance and emissions of a supercharged producer gas-diesel dual fuel engine. SAE technical paper 2009-01-1848
- Scott Guerry E, Raihan Mostafa S, Srinivasan Kalyan K et al (2016) Injection timing effects on partially premixed diesel-methane dual fuel low temperature combustion. *Appl Energy* 162 (1):99–113
- Splitter D, Kokjohn S, Rein K, Hanson R, Sanders S, Reitz R (2010) An optical investigation of ignition processes in fuel reactivity controlled PCCI combustion. SAE paper 2010-01-0345
- Srivastava DK, Dharamshi K, Agarwal AK (2011) Flame kernel characterization of laser ignition of natural gas–air mixture in a constant volume combustion chamber. *Opt Lasers Eng* 49:1201–1209
- Starikovskaia SM (2006) Plasma assisted ignition and combustion. *J Phys D* 39:265–299
- Starikovskii AY (2005) Plasma supported combustion. *Proc Comb Inst* 30:2405–2417
- Tamagna D, Gentili R, Ra Y, Reitz RD (2008) Multidimensional simulation of the influence of fuel mixture composition and injection timing in gasoline- diesel dual-fuel applications. SAE technical paper 2008-01-0031
- Tomita E, Kawahara N, Piao Z, Yamaguchi R (2002) Effects of EGR and early injection of diesel fuel on combustion characteristics and exhaust emissions in a methane dual-fuel engine. SAE technical paper 2002-01-2723
- Tomita E, Kawahara N, Kinoshita Y, Komoda T, Sakane A (2004) Combustion characteristics and performance of supercharged single cylinder natural gas engine ignited with pilot injection of diesel fuel. In: FISITA 2004, World Automotive Congress, Paper F2004V229
- Tomita E, Fukatani N, Kawahara N, Maruyama K (2007) Combustion in a supercharged biomass gas engine with micro-pilot ignition-effects of injection pressure and amount of diesel fuel. *J KONES Powertrain Transport* 14(2):513–520
- Tomita E, Harada Y, Kawahara N, Sakane A (2009) Effect of EGR on combustion and exhaust emissions in supercharged dual-fuel natural gas engine ignited with diesel fuel. SAE technical paper 2009-01-1832
- Union Gas Limited, Chemical composition of natural gas. Available <http://www.uniongas.com/aboutus/aboutng/composition.asp>. Accessed 08 July 2018
- Wagemakers AMLM, Leermakers CAJ (2012) Review on the effects of dual-fuel operation, using diesel and gaseous fuels, on emissions and performance. SAE technical paper 2012-01-0869
- Wienrotter M, Srivastava DK, Iskra K, Graf J, Kopecek H, Klausner J et al (2006) Laser ignition of engines: a realistic option. *Proc SPIE* 6053:605316
- Xu M, Cheng W, Li Z, Zhang H, An T, Meng Z (2016) Pre-injection strategy for pilot diesel compression ignition natural gas engine. *Appl Energy* 179:1185–1193
- Yang S, Reitz RD (2010) A continuous multicomponent fuel flame propagation and chemical kinetics model. *Intern Combust Engines* 132(7):072802
- Yap D, Megaritis A, Peucheret S, Wyszynski ML, Xu H. Paper presented at fuels & lubricants meeting & exhibition, Toulouse, France. SAE paper no. 2004-01-1972
- Yap D, Peucheret SM, Megaritis A, Wyszynski ML, Xu H (2006) *Int J Hydrogen Energy* 31:587–595

- Zheng J (2012) The potential of using natural gas in HCCI engines: results from zero- and multi-dimensional simulations. PhD Dissertation, Texas A&M University, College Station
- Zheng J, Caton J (2012) Effects of operating parameters on nitrogen oxides emissions for a natural gas fueled homogeneous charged compression ignition engine (HCCI): results from a thermodynamic model with detailed chemistry. *Appl Energy* 92:386–394
- Zheng QP, Zhang HM, Zhang DF (2005) A computational study of combustion in compression ignition natural gas engine with separated chamber. *Fuel* 84:1515–1523
- Zhou D, Yang W, An H, Li J, Shu C (2015) A numerical study on RCCI engine fueled by biodiesel/methanol. *Energy Convers Manage* 89:798–807
- Zoldak P, Sobiesiak A, Bergin M, Wickman D (2014) Computational study of reactivity controlled compression ignition (RCCI) combustion in a heavy-duty diesel engine using natural gas. SAE paper 2014-01-1321
- Zoldak P, Sobiesiak A, Wickman D, Bergin M (2015) Combustion simulation of dual fuel CNG engine using direct injection of natural gas and diesel. *SAE Int J Engines* 8(2):846–858